

AAU-net: An Adaptive Attention U-net for Breast Lesions Segmentation in Ultrasound Images

Gongping Chen, *Student Member, IEEE*, Yu Dai, *Member, IEEE*, Jianxun Zhang, *Member, IEEE*, and Moi Hoon Yap, *Senior Member, IEEE*

Abstract—Various deep learning methods have been proposed to segment breast lesion from ultrasound images. However, similar intensity distributions, variable tumor morphology and blurred boundaries present challenges for breast lesions segmentation, especially for malignant tumors with irregular shapes. Considering the complexity of ultrasound images, we develop an adaptive attention U-net (AAU-net) to segment breast lesions automatically and stably from ultrasound images. Specifically, we introduce a hybrid adaptive attention module, which mainly consists of a channel self-attention block and a spatial self-attention block, to replace the traditional convolution operation. Compared with the conventional convolution operation, the design of the hybrid adaptive attention module can help us capture more features under different receptive fields. Different from existing attention mechanisms, the hybrid adaptive attention module can guide the network to adaptively select more robust representation in channel and space dimensions to cope with more complex breast lesions segmentation. Extensive experiments with several state-of-the-art deep learning segmentation methods on three public breast ultrasound datasets show that our method has better performance on breast lesion segmentation. Furthermore, robustness analysis and external experiments demonstrate that our proposed AAU-net has better generalization performance on the segmentation of breast lesions. Moreover, the hybrid adaptive attention module can be flexibly applied to existing network frameworks.

Index Terms—Breast cancer segmentation, Ultrasound images, Hybrid attention, Adaptive learning, Deep learning.

I. INTRODUCTION

Breast cancer is a common female disease, which seriously threatens women's health and life [1]. Therefore, regular breast screening and diagnosis are very important to formulate treatment plans and improve survival rates. Due to the flexibility and convenience of ultrasound imaging, it has become a convention modality for breast tumors screening. Segmentation of breast ultrasound (BUS) images can help us characterize and localize breast tumors, which is one of the key steps in computer-aided diagnosis (CAD) [2]–[4]. In recent years, many deep learning methods have been proposed to segment breast lesions from ultrasound images [5]–[9].

However, complex ultrasound patterns, similar intensity distributions, variable tumor morphology and blurred boundaries seriously interfere with the segmentation accuracy of breast lesions, and even breast tumors cannot be detected, as shown in Fig. 1.

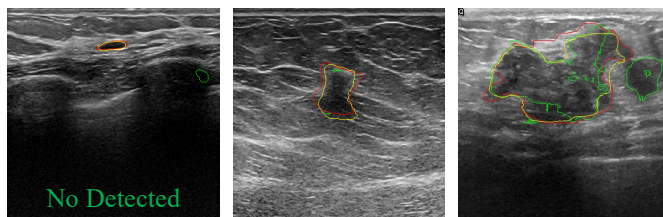


Fig. 1. Various BUS images and the segmentation results by U-net and our method. The red curve is the ground-truth boundary of the lesion. The yellow and green curves are the segmentation results of our method and U-net, respectively. It can be seen from these images that tumor morphology, blurred borders and similar surrounding tissue (background) severely affect the segmentation accuracy of breast lesions, especially for small and malignant tumors.

The powerful nonlinear learning ability makes full convolution network (FCN) and U-net have achieved great success in medical images segmentation [10]–[15]. Enlightened by this, many deep learning methods are proposed to segment breast lesions from ultrasound images [5]–[9]. In 2017, Yap *et al.* [16] are the first to systematically evaluate the impact of different FCN variants on breast lesions segmentation and achieve segmentation results that outperform traditional methods. In 2018, Almajalid *et al.* [17] improve the segmentation accuracy of U-net for breast lesions by contrast enhancement and speckle noise removal strategy. These preprocessing operations can improve network performance, but they destroy the original spatial feature distribution of objects. Moreover, Ning *et al.* [18] point out that the complex ultrasound pattern and the interference of surrounding tissues make it difficult for these simple frameworks to achieve ideal segmentation results on BUS images, as shown in Fig. 1.

To further refine the segmentation results of BUS lesions, two optimization strategies: enlarging the receptive field [19]–[21] and the attention mechanism [22]–[25] have been widely used. The dilated convolution operation is a commonly used strategy to expand the receptive field [26]–[28]. For example,

This work is supported by the National Natural Science Foundation of China Grant U1913207 and Grant 51875394. (Corresponding author: Yu Dai, e-mail: daiyu@nankai.edu.cn)

G. P. Chen, Y. Dai and J. X. Zhang are with the College of Artificial Intelligence, Nankai University, Tianjin, 300350 China (e-mail: cgp110@mail.nankai.edu.cn, daiyu@nankai.edu.cn, zhangjx@nankai.edu.cn).

M. H. Yap is with the School of Computing, Mathematics and Digital Technology, Manchester Metropolitan University, Manchester M1 5GD, U.K. (e-mail: m.yap@mmu.ac.uk).

Hu *et al.* [28] obtain the large receptive field of breast tumors by using dilated convolutions in deeper network layers. However, Xue *et al.* [25] point out that deeper convolutional layers tend to focus more on the extraction of local features, and it is difficult to obtain the true global view using dilated convolutional operations on deeper convolutional layers. Irfan *et al.* [26] develop an end-to-end semantic segmentation network using dilated convolution operations to segment breast tumors from the BUS image. Cao *et al.* [27] integrate a set of hybrid dilated convolutions into D²U-Net to alleviate the challenges posed by different lesion sizes and shapes. However, merely using dilated convolution operations to obtain a larger receptive field cannot fully cope with the perturbation caused by surrounding tissues and blurred boundaries [29]. In terms of attention mechanism, Abraham *et al.* [22] utilize an optimized attention U-net, which includes three modules of multi-scale inputs, attention U-net and deep supervision, to segment breast tumors from ultrasound images. Lee *et al.* [24] propose a channel attention module to further improve the performance of U-net for breast lesions segmentation. Since U-net uses 3×3 convolution operations, the attention mechanism can only be performed on the fixed receptive field, which limits the segmentation performance of the U-net variant network [30]. Moreover, we need to guide the network from different perspectives to handle more complex segmentation problems [25]. Xue *et al.* [25] develop a global guidance network for breast lesions segmentation by integrating a channel attention module, a spatial attention module, and a boundary detection module. However, the global features obtained on the fixed receptive field still affect the tumor segmentation accuracy. In addition, extracting lesion boundaries accurately from BUS images, especially for malignant tumors, is a challenging task.

To obtain the segmentation results of breast lesions closer to the ground-truth mask, some segmentation networks integrating dilated convolution and attention mechanisms are proposed [31], [32]. Yan *et al.* [31] propose an attention enhanced U-net (AE U-net) with hybrid dilated convolution to segment breast tumors from ultrasound images. Zhuang *et al.* [32] develop a residual dilated attention-gate U-net (RDAU-Net) to segment breast lesions by introducing dilated convolution and residual learning strategies on attention U-net. Although the performance of segmentation networks can be optimized by integrating dilated convolution and attention mechanisms, there are still some shortcomings (fixed kernel convolution and single-attention operations) that need to be further overcome.

To alleviate the above challenge, we propose a novel adaptive attention U-net to improve breast lesions segmentation by learning generic representations from BUS images. A hybrid adaptive attention module is introduced to expand the receptive field of U-net, which is able to capture receptive fields of three different scales simultaneously. Compared with conventional convolution operations with fixed receptive fields, the hybrid adaptive attention module can help the network select more robust representations from multiple perspectives. According to the previous observation [30], it ignores the effect of the dimension of the space on the target feature selection. Therefore,

we develop a spatial self-attention module to enhance object feature selection in the spatial dimension. Extensive experiments demonstrate that our adaptive attention U-net brings significant and consistent improvements in breast lesions segmentation. In this study, our main contributions are summarized as follows:

- A novel framework of adaptive attention U-net is developed for improving breast lesions segmentation. The network can not only provide different receptive fields, but also capture more robust representations from both channel and space dimensions to improve the segmentation accuracy of breast tumors.
- We design a novel hybrid adaptive attention module to improve the performance of the network to represent different objects, which can be flexibly applied to existing network frameworks.
- Extensive experiments on three public BUS datasets demonstrate that our approach consistently improves the segmentation accuracy of breast lesions, outperforming the strong baseline and the state-of-the-art medical image segmentation methods.

In the remainders of this paper, we introduce our segmentation network and loss function in Section II. The public ultrasound datasets, experimental settings and evaluation indicators is elaborated in Section III. The experimental results are presented in Section IV. Finally, our discussion and conclusions are given in Sections V and VI, respectively.

II. METHODOLOGY

The Fig. 2 is an illustration of our developed adaptive attention U-net (AAU-net) for breast lesions segmentation. Our AAU-net has the same core architecture as U-net [12] mainly including four down-sampling, four up-sampling and four skip-connections. The difference is we propose a hybrid adaptive attention module (HAAM) to replace the original convolution layer to better adapt to the segmentation of breast lesions. As shown in Fig. 2, each encoding or decoding stage consists of two HAAMs. Convolutional layers with different kernel sizes in HAAM can provide receptive fields with different scales, which can improve the adaptability of the network to different input images. Moreover, HAAM can guide the segmentation network to learn more robust representations from BUS images through channel dimension and spatial dimension constraints.

A. Hybrid Adaptive Attention Module (HAAM)

The designed HAAM mainly consists of three parts: convolutional layers with different kernel sizes, channel self-attention block, and spatial self-attention block. Specifically, the input HAAM feature map first through three parallel convolutional layers to obtain three feature maps with different receptive fields. The three convolutional layers are 3×3 convolution, 5×5 convolution, and 3×3 dilated convolution with a dilation rate of 3. The feature map captured by three convolution layers can be represented as:

$$F^3 = W_{3 \times 3} \cdot F_{input} \quad (1)$$

Finally, the feature map $F_f^{G'}$ is performed sigmoid activation to obtain the channel attention map,

$$\alpha = \delta_s(F_f^{G'}) \quad (7)$$

We let $\alpha \in [0,1]^{c \times 1 \times 1}$ and $\alpha' \in [0,1]^{c \times 1 \times 1}$ represent the channel attention maps of F^D and F^S , respectively. Each value of α / α' indicates the importance of channel information at the corresponding voxel in F^D / F^S . It is worth noting that α' is derived from α , and its value is $1-\alpha$. These two channel attention maps can help us adaptively extract more representative feature maps from receptive fields with different scales. In order to achieve automatic feature selection, we use the channel attention map α to calibrate the feature map F^G , the channel attention map α' to calibrate the feature map F^S . The feature map after channel attention map calibration can be expressed as:

$$F_C^D = \alpha \otimes F^D \quad (8)$$

$$F_C^S = \alpha' \otimes F^S \quad (9)$$

Subsequently, the feature maps $F_C^D \in \mathbb{R}^{c \times h \times w}$ and $F_C^S \in \mathbb{R}^{c \times h \times w}$ are integrated and used as the input of the next stage.

C. Spatial Self-Attention Block

As we all know, the channel attention mechanism focuses on the category of the feature, and the spatial attention mechanism focuses on the location of the feature [33]. To further improve the robustness of network representation features, we develop a novel spatial self-attention block as shown in Fig. 2 (b). The feature maps obtained by the 3×3 convolution layer and the channel self-attention block are used as the input of the spatial self-attention block. To refine the location information of the objective, we first perform a 1×1 convolution operation on the input feature map. The feature map after 1×1 convolution can be defined as:

$$F^{S1} = W_{1 \times 1} \cdot F^3 \quad (10)$$

$$F_C^{S1} = W_{1 \times 1} \cdot (F_C^S \oplus F_C^D) \quad (11)$$

where F_C^D and F_C^S denote the output of the channel self-attention block, F^3 represents the feature map obtained by performing 3×3 convolution operations on the input of HAAM. Subsequently, the feature maps fused with F^{S1} and F_C^{S1} undergo a ReLU activation $\sigma_r(\cdot)$, a 1×1 convolution operation and a sigmoid activation $\sigma(\cdot)$, to obtain the spatial attention map.

$$\beta = \sigma(W_{1 \times 1} \cdot \sigma_r(F^{S1} \oplus F_C^{S1})) \quad (12)$$

We let $\beta \in [0,1]$ and $\beta' \in [0,1]$ represent the spatial attention maps of F_C^{S1} and F^{S1} , respectively. It is worth noting that the value of β' is $1-\beta$. Each value of β / β' indicates the importance of spatial information at the corresponding voxel in F_C^{S1} / F^{S1} . To perform calibration on F_C^{S1} , β is resampled to obtain a spatial attention map with the same number of channels as F_C^{S1} . Similarly, the resample operation is performed for β' . The feature maps calibrated by β and β' can be denoted as $F_C^{S1'}$ and $F^{S1'}$, respectively. Finally, the output of the spatial self-attention block is obtained after the connected $F_C^{S1'}$ and $F^{S1'}$ are subjected to the convolution operation.

$$F_{out} = W_{1 \times 1} \cdot (F_C^{S1'} \oplus F^{S1'}) \quad (13)$$

F_{out} is also the output of the entire hybrid adaptive attention module (HAAM).

D. Loss Function

Binary cross entropy (BCE) [34] is one of the widely used loss functions in two-class image segmentation tasks, which reflects the direct difference between predicted masks and ground-truth labels. Its definition can be expressed as:

$$\ell_{BCE} = - \sum_{(i,j)} Y(i,j) \cdot \log \hat{Y}(i,j) + (1 - Y(i,j)) \cdot \log(1 - \hat{Y}(i,j)) \quad (14)$$

where $Y(i,j) \in [0,1]$ denotes the ground-truth label of the pixel (i,j) , $\hat{Y}(i,j) \in [0,1]$ represents the predict masks. In this study, we use BCE loss for the training of the network.

TABLE I
SAMPLE DISTRIBUTION OF THE THREE PUBLIC BUS DATASET.

	Benign	Malignant	Normal	Total	Cross-validation	External-validation
BUSI	437	210	133	780	True	False
Dataset B	110	53	No	163	True	True
STU	Unknow	Unknow	No	42	False	True

III. DATASETS AND EXPERIMENTAL SETTINGS

A. BUS Datasets

In this paper, we use three public BUS datasets for evaluating network performance. The first BUS dataset (denotes as BUSI) was constructed by Al-Dhabyani *et al.* [35]. The dataset contains 780 images acquired by two types of ultrasound equipment (LOGIQ E9 ultrasound and LOGIQ E9 Agile ultrasound system) in the Baheya Hospital. The average image size of these images is 500×500 pixels. The second BUS dataset used in this paper named Dataset B was created by Yap *et al.* [2]. Dataset B contains 163 images with average image size is 760×570 pixels collected by Siemens ACUSON Sequoia C512 system. The third public BUS dataset is the STU provided by Zhuang *et al.* [32]. The STU contains 42 BUS

images acquired by the Imaging Department of the First Affiliated Hospital of Shantou University using the GE Voluson E10 ultrasonic diagnostic system. Table I describes the sample distribution of these three public BUS datasets. Since the dataset STU contains too few images, it is only used as external validation data to evaluate the generalization performance of the network. Since we only focus on the segmentation of breast lesions, normal BUS images in the BUSI dataset are not exploited.

B. Experimental Settings

During training, we choose Adam optimizer to train our network. The initial learning rate of our network is 0.001. Multiple cross-validation shows that the best segmentation performance is obtained when epoch size and batch size are set to 50 and 12, respectively. Our experimental device is a PC with two NVIDIA RTX 3090 GPUs. The development environment is Ubuntu 20.04, python 3.6 and TensorFlow 2.6.0.

C. Evaluation Metrics

To quantitatively evaluate the segmentation performance of different methods on breast lesions, we use six widely used segmentation metrics. For a detailed description of the six evaluation indicators of Jaccard, Precision, Recall, Specificity, Dice and AUC, please refer to [36].

IV. EXPERIMENTAL RESULTS

In this section we first conduct ablation experiments on different components of the network. Then, we compare our method with state-of-the-art deep learning segmentation methods. Finally, the robustness of our network is analyzed.

A. Ablation Study

To evaluate the performance of different network components, we perform ablation experiments on Dataset B. In the ablation experiments, U-net is used as the benchmark network and four-fold cross-validation is performed on Dataset B. Table II shows the experimental results of different components on Dataset B. Comparing the segmentation results of U-net and ‘U-net with channel self-attention block’, we can see that adaptively selecting features from the dimension of the channel can improve the segmentation performance of the network. Compared with ‘U-net with channel self-attention block’, the design of spatial self-attention block can further improve the segmentation performance of the network, which indicates that the selection of features adaptively from the spatial dimension is more beneficial for the segmentation of

breast lesions. From Table II, we can see that HAAM enables the network to achieve the best segmentation results on Dataset B. This suggests that integrating the constraints of channel self-attention block and spatial self-attention block can help the network learn more robust representations from BUS images. It is worth noting that the above ablation experiments were performed on the large receptive field. To further evaluate the perturbation of receptive field size on segmentation performance. We first replace the 5×5 convolution with the 3×3 convolution, and then reduce the dilation rate of the 3×3 dilated convolution from 3 to 2. According to the segmentation results in the fourth row of Table II, we can conclude that the small receptive field will reduce the segmentation performance of the network, but still outperforms the original U-net. In summary, these key components designed in this paper all play a role in improving network performance.

B. Comparison with State-of-the-Art Methods

To evaluate the robustness and effectiveness of the method proposed in this paper, our method is first compared with state-of-the-art deep learning methods for segmentation of BUS images and medical images. Our comparative methods include U-net [12], SegNet [13], Att U-net [23], U-net++ [14], U-net3+ [15], Abraham *et al.* [22], SKNet [29], AE U-Net [31] and RDAU-Net [32]. To ensure the fairness of the comparison, all comparative experiments are performed on the BUSI and Dataset B datasets by four-fold cross-validation.

The quantitative evaluation of the segmentation results of BUSI and Dataset B by different segmentation methods is presented in Table III. From the experimental results in Table III, we can draw several conclusions. In general, the U-net-based variant network (such as U-net++ and U-net3+) achieves better segmentation results than the original U-net, which indicates that the use of skip-connection operations to fuse low-level features in the encoding stage with high-level features in the decoding stage is beneficial for the segmentation of breast lesions. By analyzing the segmentation results of the U-shaped network with the attention mechanism (such as Att U-net and RDAU-Net), it can be concluded that the introduction of the attention mechanism can also improve the segmentation performance of the network. Compared with the results of AE U-net and SKNet, the optimized attention mechanism can further improve the performance of the network to segment breast lesions. From the segmentation results of the method proposed by Abraham *et al.*, it can be seen that introducing the strategy of deep supervision and multi-scale inputs into Att U-net can further improve the segmentation accuracy of breast

TABLE II
THE SEGMENTATION RESULTS (MEAN \pm STD) OF DIFFERENT NETWORK COMPONENTS ON DATASET B BY FOUR-FOLD CROSS-VALIDATION.

	Jaccard	Precision	Recall	Specificity	Dice
Baseline U-net	58.44 \pm 4.26	70.27 \pm 6.11	75.32 \pm 2.85	98.44 \pm 0.40	68.20 \pm 4.23
U-net with channel self-attention block	62.76 \pm 3.60 \uparrow	74.28 \pm 4.56 \uparrow	78.45 \pm 4.11 \uparrow	98.74 \pm 0.28 \uparrow	72.37 \pm 3.29 \uparrow
U-net with spatial self-attention block	66.94 \pm 2.26 \uparrow	76.33 \pm 2.61 \uparrow	80.64 \pm 4.13 \uparrow	98.75 \pm 0.39 \uparrow	75.77 \pm 1.84 \uparrow
U-net with HAAM (Small receptive fields)	64.12 \pm 3.93 \downarrow	73.27 \pm 3.26 \downarrow	80.97 \pm 4.03 \downarrow	98.53 \pm 0.35 \downarrow	73.42 \pm 3.49 \downarrow
U-net with HAAM (Ours)	69.10\pm2.98\uparrow	78.83\pm2.40\uparrow	82.22\pm3.84\uparrow	98.82\pm0.35\uparrow	78.14\pm2.41\uparrow

TABLE III

THE SEGMENTATION RESULTS (MEAN \pm STD) OF DIFFERENT COMPETING METHODS ON BUSI AND DATASET B BY FOUR-FOLD CROSS-VALIDATION. ASTERISKS INDICATE THAT THE DIFFERENCE BETWEEN OUR METHOD AND THE COMPETING METHOD IS SIGNIFICANT USING A PAIRED STUDENT'S T-TEST. (*: $P < 0.05$).

	Method	U-net	Att U-net	RDAU-Net	U-net++	Abraham <i>et al.</i>	U-net3+	SegNet	AE U-net	SKNet	Ours
BUSI	Jaccard	57.32 \pm 3.40	59.07 \pm 2.30	59.17 \pm 2.00	62.14 \pm 2.99	61.43 \pm 2.63	62.20 \pm 2.81	62.39 \pm 2.65	62.64 \pm 1.97	64.48 \pm 2.37*	67.97\pm1.99
	Precision	70.96 \pm 2.77	69.43 \pm 1.43	67.70 \pm 3.39	71.71 \pm 3.40	73.10 \pm 3.27	71.68 \pm 2.87	71.38 \pm 2.98	73.52 \pm 3.82	75.37 \pm 3.22*	78.66\pm3.12
	Recall	72.42 \pm 5.14	77.01 \pm 2.61	76.62 \pm 1.86	78.50 \pm 1.69	77.17 \pm 3.45	78.72 \pm 2.34	79.41 \pm 3.22*	77.71 \pm 2.46	78.56 \pm 3.27	80.63\pm3.36
	Specificity	96.67 \pm 1.04	96.40 \pm 0.91	96.63 \pm 0.96	96.73 \pm 1.07	96.85 \pm 1.02	96.77 \pm 0.92	96.99 \pm 0.90	97.19 \pm 1.06	97.21 \pm 1.02*	97.75\pm0.97
	Dice	67.98 \pm 2.91	69.12 \pm 2.17	68.57 \pm 2.01	71.54 \pm 2.87	71.29 \pm 2.52	71.63 \pm 2.84	71.69 \pm 2.54	72.13 \pm 1.77	74.03 \pm 2.21*	77.21\pm2.00
Dataset B	Jaccard	58.44 \pm 4.26	59.93 \pm 4.53	58.17 \pm 4.91	61.19 \pm 5.86	63.09 \pm 3.04	65.63 \pm 5.26*	62.83 \pm 2.20	62.37 \pm 2.16	64.25 \pm 4.01	69.10\pm2.98
	Precision	70.27 \pm 6.11	70.40 \pm 6.05	70.49 \pm 4.26	68.32 \pm 5.73	73.70 \pm 5.08	73.50 \pm 6.21	71.72 \pm 1.70	72.27 \pm 1.91	75.27 \pm 6.70*	78.83\pm2.40
	Recall	75.32 \pm 2.85	76.15 \pm 4.21	73.55 \pm 5.28	79.64 \pm 3.84	79.24 \pm 1.72	80.29 \pm 3.93*	80.15 \pm 3.90	78.97 \pm 2.29	79.36 \pm 2.50	82.22\pm3.84
	Specificity	98.44 \pm 0.40	98.43 \pm 0.33	98.37 \pm 0.39	98.44 \pm 0.41	98.61 \pm 0.36	98.60 \pm 0.36	98.59 \pm 0.30	98.67 \pm 0.28	98.68 \pm 0.39*	98.82\pm0.35
	Dice	68.20 \pm 4.23	69.30 \pm 4.07	68.22 \pm 4.94	69.77 \pm 5.30	72.32 \pm 3.14	73.98 \pm 4.72*	72.16 \pm 1.52	72.23 \pm 2.14	73.53 \pm 4.05	78.14\pm2.41

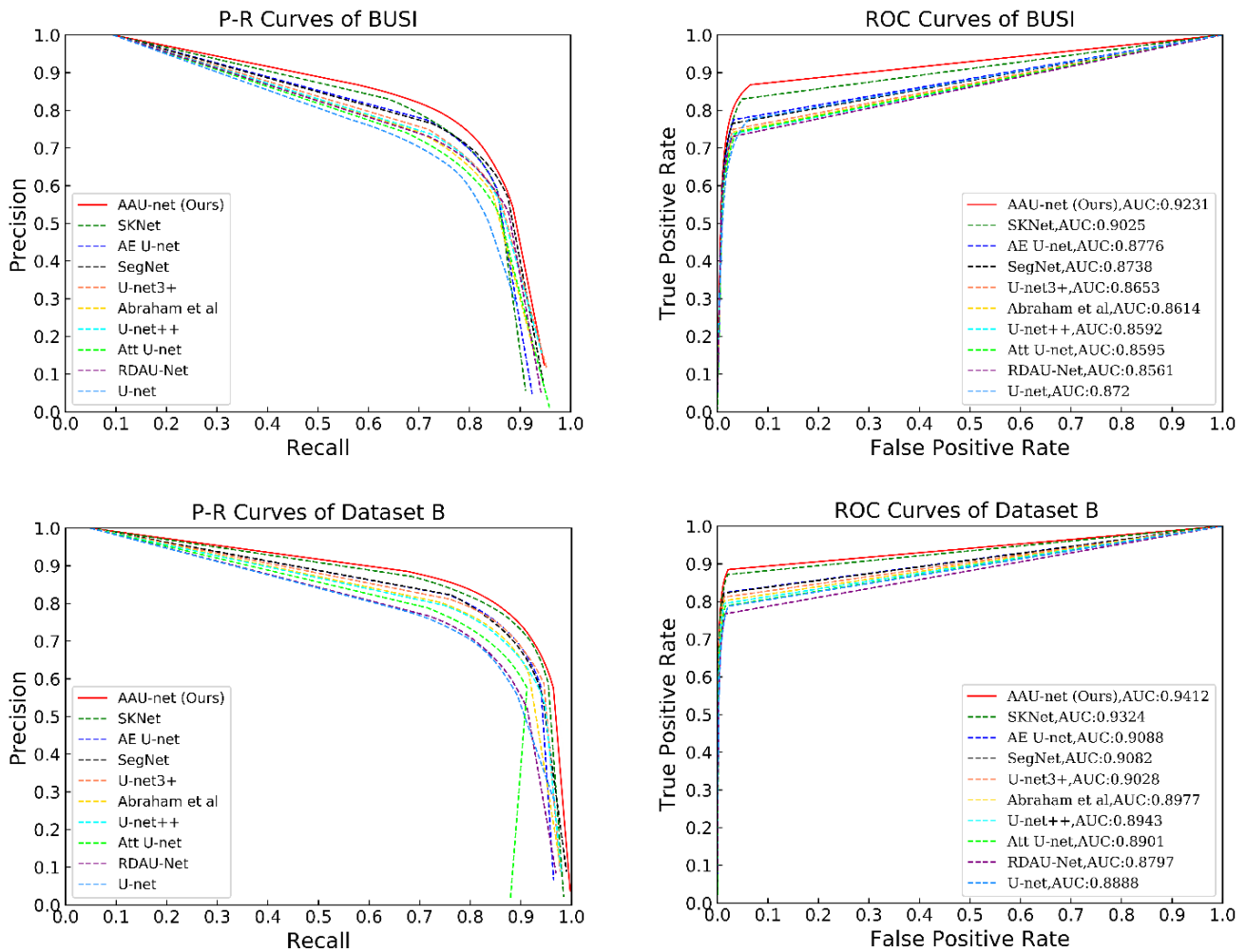


Fig. 4. P-R and ROC curves of different segmentation methods on BUSI and Dataset B.

lesions. Based on the segmentation results of SegNet, it can be seen that using the location information of the features in the U-shaped network can achieve better results than most segmentation methods. Generally speaking, SKNet achieves good performance on breast lesion segmentation among the compared methods. Compared with SKNet, the larger receptive field and spatial self-attention block introduced by our method

can effectively improve the performance of the network in segmenting breast lesions. Finally, the method proposed in this paper achieves the best segmentation performance regardless of the size of the dataset. The five evaluation index values of our method on BUSI are 67.97, 78.66, 80.63, 97.75 and 77.21, respectively. Compared to the second results, these metrics are improved by 5.4%, 4.4%, 1.5%, 0.6% and 4.3%, respectively.

Compared to the second results on Dataset B, our method improves these five metrics by 5.3%, 4.7%, 2.4%, 0.1% and 5.6%, respectively. To further demonstrate the advantages of our method, we perform paired student's t-test with the second results, and the resulting p-values ($p < 0.05$) indicates a significant difference between our method and the comparison method. In addition, we also illustration the P-R curves and ROC curves of different segmentation methods on BUSI and Dataset B in Fig. 4. The P-R curve represents the confidence level that the true positive and false positive classes are predicted correctly. The ROC curve represents the confidence level that a method predicts correctly. The AUC scores are shown in the ROC curves. Compared to other methods, our method achieves the highest AUC values on both BUSI and Dataset B. According to the comparison of P-R and ROC curves, it can be concluded that the method proposed in this paper achieves the highest confidence level on both BUSI and Dataset B segmentation.

Fig. 5 shows the visual segmentation results on BUSI and Dataset B by different methods. Based on these visual segmentation results, we can summarize four key points. According to the segmentation results of the first and second

rows, we can see that various methods have some missed detection for small breast tumors, and even fail to detect breast tumors. From the segmentation results in the first to fourth rows we can conclude that the surrounding tissue (background) with similar intensity distribution can cause serious missed detection and false detection of breast lesions. Severe heterogeneity makes breast lesions undetectable by various methods as shown in the fifth and sixth rows. Furthermore, accurate tumor contours cannot be captured from blurred or cascaded BUS images as shown in the last two rows of images. Compared with the segmentation results of other methods, our method not only effectively alleviate the perturbation of tumor size, surrounding tissue and cascade, but also achieve segmentation results that are closer to the ground-truth mask. Moreover, the method proposed in this paper can alleviate the influence of heterostructure on the segmentation results to a certain extent. Although our method still suffers from false detections and missed detections, it achieves significant improvements compared to other methods. Comprehensive evaluation results and visual effects show that our method achieves the best segmentation results with fewer missed and false detections in breast lesion segmentation.

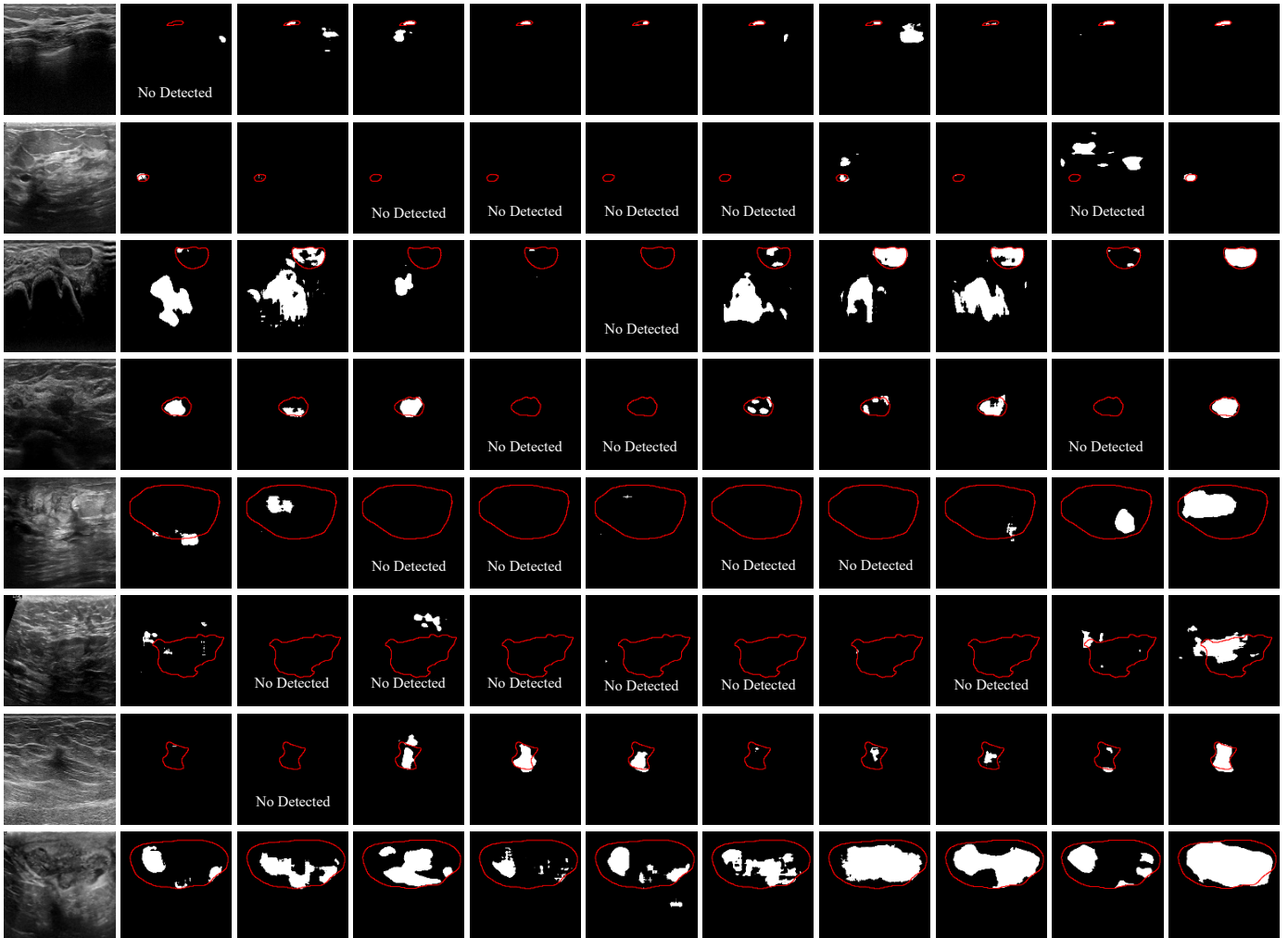


Fig. 5. Segmentation results of different methods on BUSI and Dataset B. From left to right are images of Input, U-net, Att U-net, RDAU-Net, U-net++, Abraham *et al.*, U-net3+, SegNet, AE U-net, SKNet and Ours. The red curve is the boundary of the breast lesion.

TABLE IV

THE SEGMENTATION RESULTS (MEAN \pm STD) OF BENIGN AND MALIGNANT LESIONS IN BUSI BY DIFFERENT METHODS. WE PERFORMED FOUR-FOLD CROSS-VALIDATION ON THE BENIGN LESIONS AND THREE-FOLD CROSS-VALIDATION ON THE MALIGNANT LESIONS. ASTERISKS INDICATE THAT THE DIFFERENCE BETWEEN OUR METHOD AND THE COMPETING METHOD IS SIGNIFICANT USING A PAIRED STUDENT'S T-TEST. (*: $p < 0.05$).

	Method	U-net	Att U-net	RDAU-Net	U-net3+	Abraham <i>et al.</i>	U-net++	SegNet	AE U-net	SKNet	Ours
Benign	Jaccard	61.53 \pm 3.98	65.03 \pm 2.05	64.70 \pm 2.17	67.63 \pm 1.86	66.74 \pm 2.10	68.25 \pm 2.75	67.89 \pm 3.31	67.89 \pm 1.96	69.91 \pm 2.11*	73.33\pm2.09
	Precision	74.97 \pm 2.80	75.24 \pm 1.68	72.54 \pm 1.57	75.58 \pm 2.88	76.74 \pm 2.94	75.93 \pm 3.66	76.96 \pm 3.11	77.17 \pm 3.63	79.15 \pm 2.05*	82.70\pm2.90
	Recall	73.97 \pm 5.81	79.44 \pm 2.84	79.36 \pm 0.98	81.07 \pm 1.27	79.97 \pm 1.64	81.58 \pm 1.09*	79.57 \pm 2.21	80.54 \pm 1.25	81.54 \pm 2.17	83.14\pm0.87
	Specificity	97.72 \pm 0.59	97.68 \pm 0.62	97.79 \pm 0.28	97.72 \pm 0.58	97.75 \pm 0.60	97.74 \pm 0.62	97.98 \pm 0.46	97.95 \pm 0.60	98.06 \pm 0.52*	98.39\pm0.47
	Dice	70.49 \pm 3.23	73.30 \pm 2.00	72.70 \pm 1.62	75.07 \pm 2.10	74.82 \pm 2.26	75.56 \pm 2.79	75.47 \pm 2.91	75.77 \pm 1.82	77.88 \pm 2.98*	80.88\pm2.06
Malignant	Jaccard	51.11 \pm 2.62	51.12 \pm 2.35	51.63 \pm 1.62	54.77 \pm 3.55	54.12 \pm 2.96	54.03 \pm 3.03	54.89 \pm 1.78	55.38 \pm 1.77	57.06 \pm 2.42*	60.60\pm1.70
	Precision	64.96 \pm 2.55	61.62 \pm 0.97	60.85 \pm 5.01	65.78 \pm 2.66	67.46 \pm 3.40	65.50 \pm 2.94	63.79 \pm 2.65	67.87 \pm 3.81	69.59 \pm 4.20*	72.62\pm3.13
	Recall	68.86 \pm 4.27	72.57 \pm 2.17	71.89 \pm 2.55	74.38 \pm 3.21	72.36 \pm 5.05	73.43 \pm 2.10	77.25 \pm 4.02*	72.88 \pm 3.47	73.58 \pm 6.75	76.13\pm5.66
	Specificity	93.63 \pm 1.28	93.12 \pm 1.00	93.47 \pm 1.45	93.82 \pm 1.06	93.94 \pm 1.25	93.73 \pm 1.31	94.00 \pm 1.14	94.43 \pm 1.33	94.65 \pm 1.49*	95.11\pm1.27
	Dice	63.47 \pm 2.38	62.95 \pm 2.14	62.44 \pm 2.21	66.19 \pm 3.37	65.77 \pm 2.58	65.52 \pm 2.75	65.90 \pm 1.97	66.50 \pm 1.52	68.19 \pm 2.28*	71.54\pm1.74

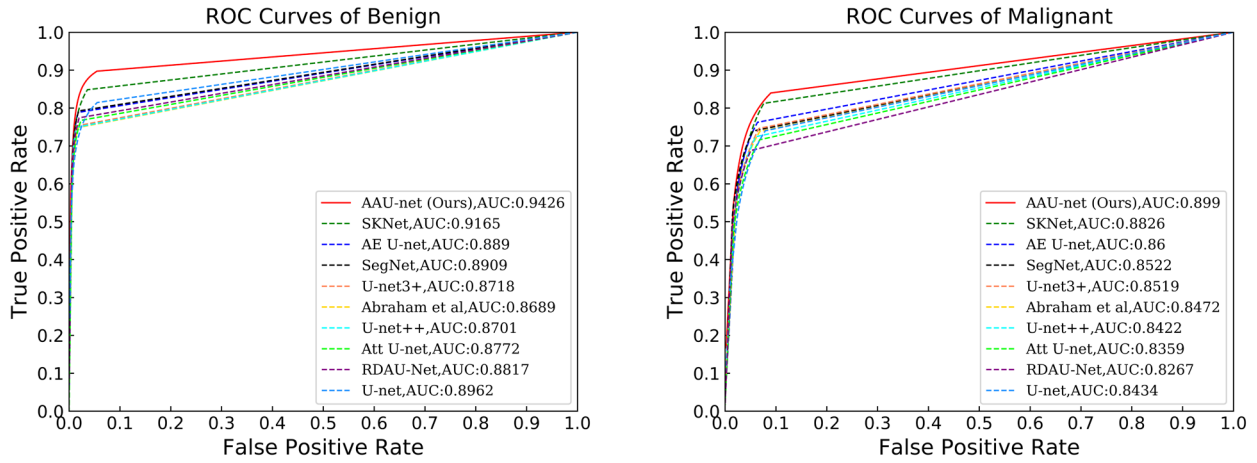


Fig. 6. ROC curves of different segmentation methods on benign and malignant breast lesions.

C. Robustness Analysis

To further evaluate the robustness of the proposed breast lesions segmentation method, we analyze the segmentation performance of different methods on benign and malignant breast tumors. Furthermore, we use STU as external validation data to evaluate the performance of different methods.

1) Robustness on Benign and Malignant Lesions Segmentation

Compared with benign lesions, malignant lesions have irregular shapes and blurred borders. In addition, the intensity distribution is more heterogeneous in malignant lesions compared to benign lesions. We conduct comparative experiments on benign and malignant BUSI images of BUSI to evaluate the robustness of the network to segment malignant and benign lesions. We perform four-fold cross-validation on benign images and three-fold cross-validation on malignant images. Table IV presents the segmentation results of different methods on malignant and benign breast lesions. Obviously, our method achieves higher scores on the segmentation of both benign and malignant lesions. Moreover, the p-value compared to the second result indicates that our method has a significant improvement in segmentation accuracy. Furthermore, we can observe two points from Table III and Table IV. First, the

segmentation accuracy of malignant lesions is inferior to benign lesions. This is well understood that malignant lesions are more diverse and complex than benign lesions. Second, there is no obvious fluctuation in the ranking of various segmentation methods, which indicates that the performance of various methods is relatively stable. In Fig. 6 we draw the ROC curves of different segmentation methods on benign and malignant breast lesions to further demonstrate the confidence level of our method. According to the ROC curves, we can clearly find that our method not only achieves convincing results on benign lesions, but also achieves the most competitive performance on the segmentation of malignant lesions.

2) External Validation

Due to the differences between different sites, there are large differences between the collected data [18]. These differences can cause the model to perform well on the training dataset, but not perform well on the external data. To further evaluate the robustness of the proposed method in this paper, we use STU as external data to test the models trained on Dataset B by different methods. Compared with BUSI, Dataset B has a smaller number of samples. Therefore, comparative analysis on the smaller dataset (Dataset B) can better reflect the superiorities of different methods. The segmentation results of

TABLE V

SEGMENTATION RESULTS (MEAN \pm STD) OF DIFFERENT COMPETING METHODS ON THE EXTERNAL VALIDATION DATASET STU BY FOUR-FOLD CROSS-VALIDATION.

	Method	Att U-net	U-net	U-net++	RDAU-Net	Abraham <i>et al.</i>	U-net3+	SegNet	AE U-net	SKNet	Ours
STU on Dataset B	Jaccard	52.65 \pm 2.29	58.90 \pm 3.75	59.18 \pm 4.21	60.11 \pm 3.02	58.11 \pm 3.24	61.51 \pm 1.78	62.70 \pm 3.09	62.46 \pm 2.44	66.94 \pm 3.15	68.99\pm3.29
	Precision	59.26 \pm 2.86	66.27 \pm 5.46	64.86 \pm 5.36	63.49 \pm 2.86	66.05 \pm 3.69	67.12 \pm 2.22	66.57 \pm 3.05	66.79 \pm 2.95	71.99 \pm 4.08	74.91\pm3.18
	Recall	86.35 \pm 1.29	86.88 \pm 1.60	89.67 \pm 1.59	91.37 \pm 1.07	86.17 \pm 0.99	89.96 \pm 1.01	91.36 \pm 0.38	91.24 \pm 0.42	91.44 \pm 1.08	92.12\pm0.75
	Specificity	93.41 \pm 0.41	94.54 \pm 0.74	94.33 \pm 0.83	94.70 \pm 0.45	94.35 \pm 0.47	94.49 \pm 0.31	95.04 \pm 0.49	95.00 \pm 0.39	95.40 \pm 0.51	95.94\pm0.71
	Dice	65.19 \pm 2.73	71.41 \pm 3.67	70.70 \pm 4.19	72.40 \pm 2.74	70.32 \pm 3.01	72.96 \pm 1.69	73.50 \pm 3.62	74.41 \pm 2.30	78.29 \pm 3.05	80.23\pm2.60

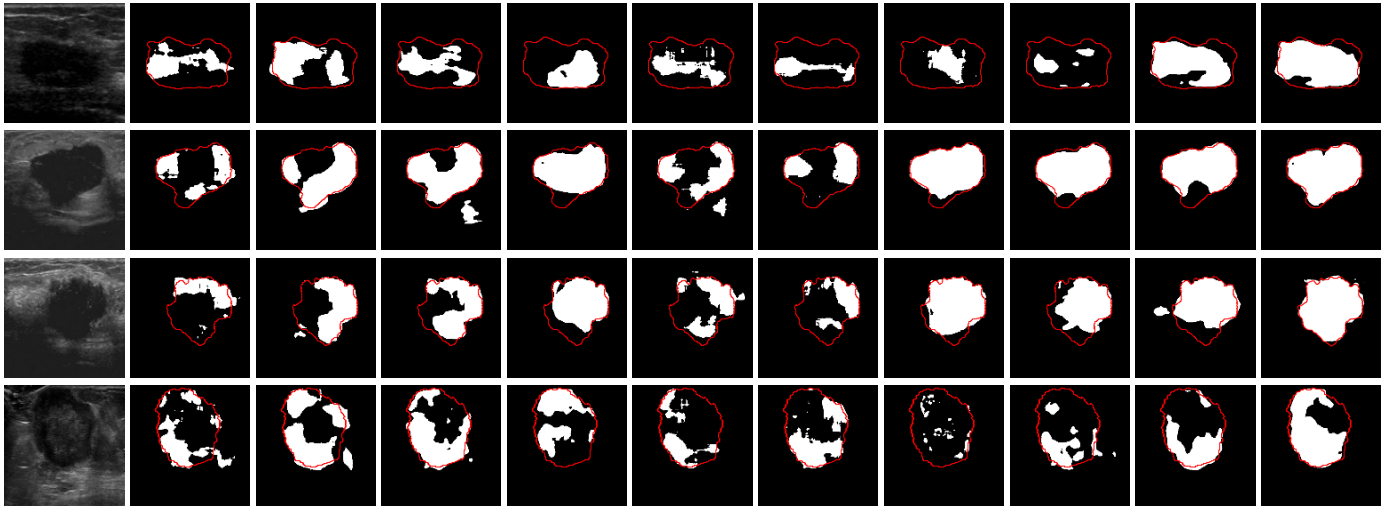


Fig. 7. Illustration of the segmentation results of different methods on STU. From left to right are images of Input, Att U-net, U-net, U-net++, RDAU-Net, Abraham *et al.*, U-net3+, SegNet, AE U-net, SKNet and Ours. The red curve is the boundary of the breast tumor.

various methods on the external validation dataset STU are presented in Table V. Similar to the above analysis, our method still achieves the best results on five evaluation metrics. This shows that the method proposed in this paper has better robustness compare to other methods, and is more suitable for the segmentation of breast lesions. SegNet, AE U-net and SKNet still obtain competitive results among the compared methods, which indicates that these three methods have certain potential in breast lesion segmentation. It is worth noting that the segmentation performance of Att U-net and U-net++ is degraded on STU. The occurrence of this phenomenon may be caused by their poor generalization ability. Fig. 7 shows the segmentation of different methods on the external validation dataset STU. Visually, our method achieves the best segmentation results with fewer missed and false detections. From the first and fourth rows, it can be seen that the heterostructure affects the segmentation accuracy of various methods. Fortunately, our method is able to mitigate their perturbations. Overall, our method achieves the best segmentation results on external validation data STU.

V. DISCUSSION

In this study, we propose a novel adaptive attention component to face the challenge of BUS images segmentation. To evaluate the effectiveness of the developed components, we first perform the ablation studies. According to the experimental results in Table II, we can clearly see that the components designed in this paper can effectively improve the segmentation accuracy of breast lesions. In addition, we can

also conclude that the components proposed in this paper (such as channel self-attention block, spatial self-attention block and hybrid adaptive attention module) can be flexibly applied to existing network frameworks. Then, we conduct comparative experiments on public datasets using six commonly used evaluation metrics with state-of-the-art deep learning methods. Experimental results show that our method has very superior performance on breast lesion segmentation. The P-R and ROC curves of the segmentation results show that our method have higher confidence level. Especially, the comparison with SKNet [29] fully illustrates the feasibility and superiority of the hybrid adaptive attention module in dealing with the challenge of breast lesion segmentation. In addition, the p-value obtained based on t-test also reflects the advantages of our method in segmenting BUS images. Finally, we further validate the robustness of our method on breast lesion segmentation. From the robustness analysis experiments we can see that although the advantages of our method are reduced, it still achieves better segmentation performance than other compared methods.

Although the method proposed in this paper has achieved good performance on breast lesion segmentation, it can be seen from Fig. 5 and Fig. 7 that our method still has some shortcomings. (1) For more complex BUS images segmentation, our method still needs to be further optimized to reduce the false detection and missed detection rate. (2) How to obtain accurate object contours is still a challenge task. Therefore, we will conduct more in-depth research on breast lesions segmentation in the future.

VI. CONCLUSION

To better address the challenge of breast tumor segmentation, we design a novel hybrid adaptive attention module (HAAM) and use it to construct an adaptive attention U-net (AAU-net) for breast lesions segmentation. The hybrid adaptive attention module can guide the network to adaptively select more robust representation in both channel and space dimensions to cope with more complex breast lesions segmentation. Extensive experiments (comparative experiments, robustness analysis and external validation) with several state-of-the-art deep learning segmentation methods demonstrate that our method has better performance on breast lesion segmentation.

REFERENCES

- [1] S. Y. Shin, S. Lee, I. D. Yun, S. M. Kim, and K. M. Lee, "Joint weakly and semi-supervised deep learning for localization and classification of masses in breast ultrasound images," *IEEE Trans. Med. Imaging*, vol. 38, no. 3, pp. 762–774, 2018.
- [2] M. H. Yap, M. Goyal, F. Osman, R. Martí, E. Denton, A. Juette, and R. Zwiggelaar, "Breast ultrasound region of interest detection and lesion localisation," *Artif. Intell. Med.*, vol. 107, no. August 2019, p. 101880, 2020.
- [3] M. Xian, Y. Zhang, H.-D. Cheng, F. Xu, B. Zhang, and J. Ding, "Automatic breast ultrasound image segmentation: A survey," *Pattern Recognit.*, vol. 79, pp. 340–355, 2018.
- [4] Q. Huang, Y. Luo, and Q. Zhang, "Breast ultrasound image segmentation: a survey," *Int. J. Comput. Assist. Radiol. Surg.*, vol. 12, no. 3, pp. 493–507, 2017.
- [5] E. H. Houssein, M. M. Emam, A. A. Ali, and P. N. Suganthan, "Deep and machine learning techniques for medical imaging-based breast cancer: A comprehensive review," *Expert Syst. Appl.*, vol. 167, p. 114161, 2021.
- [6] J. Bai, R. Posner, T. Wang, C. Yang, and S. Nabavi, "Applying deep learning in digital breast tomosynthesis for automatic breast cancer detection: A review," *Med. Image Anal.*, vol. 71, p. 102049, 2021.
- [7] L. Abdelrahman, M. Al Ghamdi, F. Collado-Mesa, and M. Abdel-Mottaleb, "Convolutional neural networks for breast cancer detection in mammography: A survey," *Comput. Biol. Med.*, vol. 131, p. 104248, 2021.
- [8] C. Chen, Y. Wang, J. Niu, X. Liu, Q. Li, and X. Gong, "Domain Knowledge Powered Deep Learning for Breast Cancer Diagnosis Based on Contrast-Enhanced Ultrasound Videos," *IEEE Trans. Med. Imaging*, vol. 40, no. 9, pp. 2439–2451, 2021.
- [9] Y. Wang, N. Wang, M. Xu, J. Yu, C. Qin, X. Luo, X. Yang, T. Wang, A. Li, and D. Ni, "Deeply-supervised networks with threshold loss for cancer detection in automated breast ultrasound," *IEEE Trans. Med. Imaging*, vol. 39, no. 4, pp. 866–876, 2019.
- [10] M. Xian, Y. Zhang, and H.-D. Cheng, "Fully automatic segmentation of breast ultrasound images based on breast characteristics in space and frequency domains," *Pattern Recognit.*, vol. 48, no. 2, pp. 485–497, 2015.
- [11] J. Long, E. Shelhamer, and T. Darrell, "Fully convolutional networks for semantic segmentation," in *Proceedings of the IEEE conference on computer vision and pattern recognition*, 2015, pp. 3431–3440.
- [12] O. Ronneberger, P. Fischer, and T. Brox, "U-net: Convolutional networks for biomedical image segmentation," in *International Conference on Medical image computing and computer-assisted intervention*, 2015, pp. 234–241.
- [13] V. Badrinarayanan, A. Kendall, and R. Cipolla, "SegNet: A Deep Convolutional Encoder-Decoder Architecture for Image Segmentation," *IEEE Trans Pattern Anal Mach Intell*, vol. 39, no. 12, pp. 2481–2495, 2017.
- [14] Z. Zhou, M. Siddiquee, N. Tajbakhsh, and J. Liang, "UNet++: Redesigning Skip Connections to Exploit Multiscale Features in Image Segmentation," *IEEE Trans. Med. Imaging*, vol. 39, no. 6, pp. 1856–1867, 2020.
- [15] H. Huang, L. Lin, R. Tong, H. Hu, and J. B. T.-I. 2020-2020 I. I. C. on A. Wu Speech and Signal Processing (ICASSP), "UNet 3+: A Full-Scale Connected UNet for Medical Image Segmentation," 2020.
- [16] M. H. Yap, G. Pons, J. Martí, S. Ganau, M. Sentís, R. Zwiggelaar, A. K. Davison, and R. Martí, "Automated Breast Ultrasound Lesions Detection Using Convolutional Neural Networks," *IEEE J. Biomed. Heal. Informatics*, vol. 22, no. 4, pp. 1218–1226, 2018.
- [17] R. Almajalid, J. Shan, Y. Du, and M. Zhang, "Development of a deep-learning-based method for breast ultrasound image segmentation," in *2018 17th IEEE International Conference on Machine Learning and Applications (ICMLA)*, 2018, pp. 1103–1108.
- [18] Z. Ning, S. Zhong, Q. Feng, W. Chen, and Y. Zhang, "SMU-Net: Saliency-guided Morphology-aware U-Net for Breast Lesion Segmentation in Ultrasound Image," *IEEE Trans. Med. Imaging*, 2021.
- [19] H. Zhao, J. Shi, X. Qi, X. Wang, and J. Jia, "Pyramid scene parsing network," in *Proceedings of the IEEE conference on computer vision and pattern recognition*, 2017, pp. 2881–2890.
- [20] L. C. Chen, G. Papandreou, I. Kokkinos, K. Murphy, and A. L. Yuille, "DeepLab: Semantic Image Segmentation with Deep Convolutional Nets, Atrous Convolution, and Fully Connected CRFs," *IEEE Trans Pattern Anal Mach Intell*, vol. 40, no. 4, pp. 834–848, 2018.
- [21] G. Chen, J. Yin, Y. Dai, J. Zhang, X. Yin, and L. Cui, "A novel convolutional neural network for kidney ultrasound image segmentation," *Comput. Methods Programs Biomed.*, vol. 218, p. 106712, 2022.
- [22] N. Abraham and N. M. B. T.-2019 I. 16th I. S. on B. I. (ISBI) Khan, "A Novel Focal Tversky Loss Function With Improved Attention U-Net for Lesion Segmentation," 2019.
- [23] O. Oktay, J. Schlemper, L. Le Folgoc, M. Lee, M. Heinrich, K. Misawa, K. Mori, S. McDonagh, N. Y. Hammerla, B. Kainz, B. Glocker, and D. Rueckert, "Attention U-Net: Learning Where to Look for the Pancreas," no. Midl, 2018.
- [24] H. Lee, J. Park, and J. Y. Hwang, "Channel attention module with multiscale grid average pooling for breast cancer segmentation in an ultrasound image," *IEEE Trans. Ultrason. Ferroelectr. Freq. Control*, vol. 67, no. 7, pp. 1344–1353, 2020.
- [25] C. Xue, L. Zhu, H. Fu, X. Hu, X. Li, H. Zhang, and P. Heng, "Global guidance network for breast lesion segmentation in ultrasound images," *Med. Image Anal.*, vol. 70, p. 101989, 2021.
- [26] R. Irfan, A. A. Almazroi, H. T. Rauf, R. Damaševičius, E. A. Nasr, and A. E. Abdelgawad, "Dilated semantic segmentation for breast ultrasonic lesion detection using parallel feature fusion," *Diagnostics*, vol. 11, no. 7, p. 1212, 2021.
- [27] X. Cao, H. Chen, Y. Li, Y. Peng, S. Wang, and L. Cheng, "Dilated densely connected U-Net with uncertainty focus loss for 3D ABUS mass segmentation," *Comput. Methods Programs Biomed.*, vol. 209, p. 106313, 2021.
- [28] Y. Hu, Y. Guo, Y. Wang, J. Yu, J. Li, S. Zhou, and C. Chang, "Automatic tumor segmentation in breast ultrasound images using a dilated fully convolutional network combined with an active contour model," *Med. Phys.*, vol. 46, no. 1, pp. 215–228, 2019.
- [29] M. Byra, P. Jarosik, A. Szubert, M. Galperin, H. Ojeda-Fournier, L. Olson, M. O'Boyle, C. Comstock, and M. Andre, "Breast mass segmentation in ultrasound with selective kernel U-Net convolutional neural network," *Biomed. Signal Process. Control*, vol. 61, 2020.
- [30] X. Li, W. Wang, X. Hu, and J. Yang, "Selective kernel networks," in *Proceedings of the IEEE/CVF Conference on Computer Vision and Pattern Recognition*, 2019, pp. 510–519.
- [31] Y. Yan, Y. Liu, Y. Wu, H. Zhang, Y. Zhang, and L. Meng, "Accurate segmentation of breast tumors using AE U-net with HDC model in ultrasound images," *Biomed. Signal Process. Control*, vol. 72, no. PA, p. 103299, 2022.
- [32] Z. Zhuang, N. Li, A. N. Joseph Raj, V. G. V Mahesh, and S. Qiu, "An RDAU-NET model for lesion segmentation in breast ultrasound images," *PLoS One*, vol. 14, no. 8, p. e0221535, 2019.
- [33] S. Woo, J. Park, J.-Y. Lee, and I. S. Kweon, "Cbam: Convolutional block attention module," in *Proceedings of the European conference on computer vision (ECCV)*, 2018, pp. 3–19.
- [34] P.-T. De Boer, D. P. Kroese, S. Mannor, and R. Y. Rubinstein, "A tutorial on the cross-entropy method," *Ann. Oper. Res.*, vol. 134, no. 1, pp. 19–67, 2005.
- [35] W. Al-Dhabyani, M. Goma, H. Khaled, and A. Fahmy, "Dataset of breast ultrasound images," *Data Br.*, vol. 28, p. 104863, 2020.
- [36] G. Chen, Y. Dai, R. Li, Y. Zhao, L. Cui, and X. Yin, "SDFNet: Automatic segmentation of kidney ultrasound images using multi-scale low-level structural feature," *Expert Syst. Appl.*, vol. 185, no. March, p. 115619, 2021.